

Image Registration Based on Low Rank Matrix: Rank-Regularized SSD

Aboozar Ghaffari and Emad Fatemizadeh

Abstract— Similarity measure is a main core of image registration algorithms. Spatially varying intensity distortion is an important challenge, which affects the performance of similarity measures. Correlation among the pixels is the main characteristic of this distortion. Similarity measures such as sum-of-squared-differences (SSD) and mutual information ignore this correlation; hence, perfect registration cannot be achieved in the presence of this distortion. In this paper, we model this correlation with the aid of the low rank matrix theory. Based on this model, we compensate this distortion analytically and introduce rank-regularized SSD (RRSSD). This new similarity measure is a modified SSD based on singular values of difference image in mono-modal imaging. In fact, image registration and distortion correction are performed simultaneously in the proposed model. Based on our experiments, the RRSSD similarity measure achieves clinically acceptable registration results, and outperforms other state-of-the-art similarity measures, such as the well-known method of residual complexity.

Index Terms— Image registration, similarity measure, low rank matrix theory, sum-of-squared-differences, spatially varying intensity distortion.

I. INTRODUCTION

IMAGE registration is spatial alignment of two or more images in a wide range of applications such as remote sensing, computer assisted surgery, and medical image analysis and processing [1]. In general, registration algorithms can be categorized as either intensity based or feature based [1]. The feature based methods use the alignment between the extracted features (such as landmark, histogram, Gabor filter and etc.) in two images [2]. In this category, feature matching is an important step which affects the performance of registration approaches [3]–[5]. The simplest feature is image intensity which is directly used in the intensity based method via similarity measure such as sum-of-squared-differences (SSD), correlation coefficient (CC), normalized cross correlation (NCC) [6], correlation ratio (CR) [7], mutual information (MI) [8]–[10], correntropy measure [11] and manifold based measure [12]–[14]. The similarity measure quantifies the matching of two images. Three main components of this category are similarity measure, spatial transform and optimization technique.

Manuscript received May 29, 2017; revised August 8, 2017; accepted August 16, 2017. Date of publication August 25, 2017; date of current version December 29, 2017. (Corresponding author: Aboozar Ghaffari.)

The authors are with the Department of Electrical Engineering, Sharif University of Technology, Tehran 11365-11155, Iran (e-mail: aboozar412@gmail.com; fatemizadeh@sharif.edu).

Color versions of one or more of the figures in this paper are available online at <http://ieeexplore.ieee.org>.

Digital Object Identifier 10.1109/TMI.2017.2744663

Spatially varying intensity distortion is an important challenge in a wide range of image processing fields such as segmentation, face recognition, object detection and image registration. Two examples of this distortion are bias field in brain magnetic resonance imaging (MRI) [1] and illumination variations in geometric photos [15]. In intensity based image registration, defining an appropriate similarity measure plays an important role to overcome this challenge. Traditional similarity measures such as SSD, CC, CR, and MI assume the pixel-by-pixel independence and stationary image [16]. Hence, these measures have poor performance in the presence of correlated noise. To resolve this issue, the idea is to model this distortion appropriately. Based on this idea, many researchers proposed many different models. One of the complicated probability models is Markov random fields (MRF) which is used to model the mentioned distortion [17]. One group of similarity measures such as regional mutual information (RMI) [18] and conditional MI (cMI) [19] is based on the assumption of constant spatially-varying intensity distortion within a small neighbourhood around each pixel. In [20], a method based on this assumption is proposed with local linear model. Also in [21], this idea has been used via total variation to measure the smoothness of the distortion. The well-known similarity measure of residual complexity (RC) uses the probability distribution $\exp(-\lambda \|\mathbf{PS}\|^2)$ to model spatially varying intensity distortion \mathbf{S} where \mathbf{P} is a linear operator [22]–[24]. Recently, authors modelled this distortion using sparse representation in the transform domain, such as discrete cosine transform (DCT) and wavelet [11], [25], [26]. Based on this sparse model, sparse induced similarity measure (SISM) which measures the sparseness of the difference image in the transform domain, was proposed [11]. Authors also proposed a robust similarity measure based on the low rank theory in the presence of this distortion [27]. Rank induced similarity measure (RISM) uses the sparse representation of this distortion in the domain of singular value decomposition (SVD) [27]. In other word, the rank of difference image is used as a similarity measure. As the matrix rank is sensitive in the presence of Gaussian noise, RISM is proposed with the aid of the effective rank definition [28] and the smoothed rank function [29]. RISM measures the sparseness of singular values of difference image. In summary, two similarity measures of SISM and RISM are sparsity measures in the different domains of transform and singular values, respectively.

Recently, the low rank matrix recovery became one of the famous tools in many applications of signal and image processing such as image registration [27],

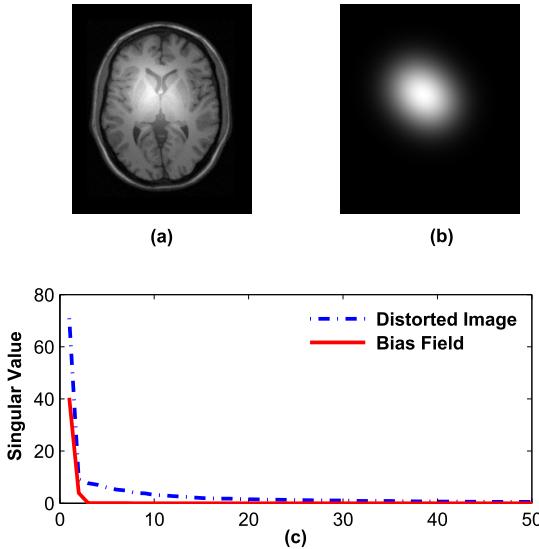


Fig. 1. (a) and (b) MRI image with spatially varying intensity distortion and bias field, respectively; (c) Singular values of spatially-varying intensity distortion (bias field) and distorted image.

matrix completion [29]–[31], alignment of linearly correlated images [32], [33], robust principal component analysis (RPCA) [34], [35] and extraction of low rank texture [36].

In this paper, we use the theory of low rank matrix recovery to model the spatially varying intensity distortion. As the pixels of the spatially varying intensity distortion are correlated, this correlation of pixels is modelled by a low rank matrix in the present paper. In Section II, based on this model, we regularize SSD with the constraint of low rank matrix, and compensate the spatially varying intensity distortion analytically. Finally, we introduce the new similarity measure of Rank-Regularized SSD (RRSSD) which is robust to spatially varying intensity distortion. Section III provides experimental results. Finally, in Section IV, we conclude and point out future work direction image.

II. THE MAIN IDEA AND THE PROPOSED APPROACH

In this section, to overcome the challenge of spatially varying intensity distortion, we propose a new similarity measure based on the low rank matrix theory. Here, we assume the following intensity relation among reference image $\mathbf{R} \in \mathbb{R}^{n \times m}$, floating image $\mathbf{F}(T) \in \mathbb{R}^{n \times m}$ and spatially varying intensity distortion $\mathbf{S} \in \mathbb{R}^{n \times m}$:

$$\mathbf{R} = \mathbf{F}(T) + \mathbf{S} + \eta \quad (1)$$

where T is a geometric transform for registering the reference \mathbf{R} and floating \mathbf{F} images. $\eta \in \mathbb{R}^{n \times m}$ is zero mean white Gaussian noise with variance ν_n^2 .

The mathematical definition of SSD is $\|\mathbf{R} - \mathbf{F}(T)\|_F^2$ where $\|\mathbf{X}\|_F = \sqrt{\sum_{i,j} x_{ij}^2}$ is the Frobenius norm. This similarity measure is optimal in the presence of Gaussian noise from the maximum a posteriori (MAP) perspective when $\mathbf{S} = \mathbf{0}$ [16]. SSD is not an appropriate similarity measure in the presence of spatially varying distortion because of pixel by pixel dependency of \mathbf{S} . In this paper, we use the low rank matrix to model this distortion, i.e. $\text{rank}(\mathbf{S}) \ll \min(n, m)$. Fig. 1 presents an

example showing the compactness of singular values for this distortion. In other words this image distortion is a low rank matrix.

A. Rank Based Similarity Measure: Rank-Regularized SSD

Here, we regularize SSD with the low rank model to compensate the spatially varying intensity distortion as the following rank-regularized SSD (RRSSD) problem:

$$\begin{aligned} \text{RRSSD} : \min_{T, S} & \|\mathbf{R} - \mathbf{F}(T) - \mathbf{S}\|_F^2 \\ \text{subject to } & \text{rank}(\mathbf{S}) \ll \min\{n, m\} \end{aligned} \quad (2)$$

In the above formulation, the estimation of geometric transform T is achieved simultaneously with the correction of distortion \mathbf{S} . To solve this optimization problem, we consider the Lagrangian form of RRSSD:

$$\text{RRSSD}_L : \min_{T, S} \frac{1}{2} \|\mathbf{R} - \mathbf{F}(T) - \mathbf{S}\|_F^2 + \lambda \text{rank}(\mathbf{S}) \quad (3)$$

where $\lambda > 0$ quantifies trade-off between rank and SSD. In this paper, our goal is to introduce a new similarity measure which has a closed-form solution depending on the two images \mathbf{R} and $\mathbf{F}(T)$. Hence, we must analytically solve the RRSSD_L problem for \mathbf{S} and eliminate it from the objective function of RRSSD_L . To do this, we suppose that the geometric transform T is fixed, the RRSSD problem will be a problem of low rank approximation.

The rank of matrix \mathbf{S} is equal to the number of non-zero singular values of \mathbf{S} . Hence, the matrix rank is too sensitive in the presence of noise [37]. Therefore, the minimization of RRSSD_L is complicated, and it does not have an analytical solution of \mathbf{S} . To resolve this problem, researchers proposed to replace rank with other functions [29]–[31]. One example is that the rank function is replaced with the following form:

$$G_\alpha(\mathbf{S}) = \sum_i f_\alpha(\sigma_{si}) \quad (4)$$

where σ_{si} is the i^{th} singular value of \mathbf{S} , and $f_\alpha(x) : \mathbb{R} \rightarrow \mathbb{R}$ is a continuous function. Two special cases of this model are the nuclear norm $\|\mathbf{S}\|_* = \sum_i \sigma_{si}$ (i.e. $f_\alpha(x) = x$) [30], [31], and the smoothed rank function based on the smoothing functions such as $f_\alpha(x) = 1 - \exp(-x^2/2\alpha^2)$ and $f_\alpha(x) = \frac{x^2}{x^2 + \alpha^2}$ [29].

Our special interest is the function $f_\alpha(x) = \frac{x^2}{x^2 + \alpha^2}$ in this paper. When $\alpha \rightarrow 0$ for this function, $G_\alpha(\mathbf{S})$ is equal to $\text{rank}(\mathbf{S})$ [29]. Note that defining an appropriate smoothing function $f_\alpha(x)$ to achieve better performance of image registration is an important task, and we will pursue further in our future study. Now, defining a matrix $\mathbf{D}_T = \mathbf{R} - \mathbf{F}(T)$ and replacing the rank function in the RRSSD_L problem with $G_\alpha(\mathbf{S})$, the following low rank matrix approximation is obtained:

$$\text{RRSSD}_{LG} : \min_{\mathbf{S}} \frac{1}{2} \|\mathbf{D}_T - \mathbf{S}\|_F^2 + \lambda G_\alpha(\mathbf{S}) \quad (5)$$

Let $\mathbf{D}_T = \mathbf{U} \text{Diag}\{\sigma_1, \sigma_2, \dots, \sigma_{\min(n,m)}\} \mathbf{V}^T$ be the singular value decomposition (SVD) of \mathbf{D}_T in which $\sigma_1 \geq \sigma_2 \geq \dots \geq \sigma_{\min(n,m)} \geq 0$ are the singular values, and the columns

of \mathbf{U} and \mathbf{V} are the singular vectors. Recently in [38], Zhou et al show that the optimal solution of $RRSSD_{LG}$ (\mathbf{S}) shares the same singular vectors as \mathbf{D}_T and its ordered singular values are the solution to

$$\min_{\sigma_{si}} \frac{1}{2}(\sigma_{si} - \sigma_i)^2 + \lambda f_\alpha(\sigma_{si}), \quad i = 1, \dots, \min(n, m) \quad (6)$$

Before solving this optimization problem, in the following Lemma, we investigate the convexity condition of the function $J_{\lambda, \alpha}(x) = \frac{1}{2}(x - a)^2 + \lambda \frac{x^2}{x^2 + \alpha^2}$. The proof of this Lemma is given in the Appendix.

Lemma 1: Let $J_{\lambda, \alpha}(x) = \frac{1}{2}(x - a)^2 + \lambda \frac{x^2}{x^2 + \alpha^2}$ be an one dimension function, if $\lambda \leq 2\alpha^2$, then the function $J_{\lambda, \alpha}(x)$ be convex.

To obtain the optimal solution of the problem (6), according to the above lemma we assume that the function $\frac{1}{2}(\sigma_{si} - \sigma_i)^2 + \lambda f_\alpha(\sigma_{si})$ is convex, on the other hand $\lambda \leq 2\alpha^2$. Hence, by differentiating this cost function with respect to σ_{si} and equating the derivative to zero, we obtain

$$\sigma_{si} + \lambda f'_\alpha(\sigma_{si}) = \sigma_i, \quad i = 1, \dots, \min(n, m) \quad (7)$$

The above equation has the concept of the singular value thresholding. The following properties of the equation (7) are interesting and useful to illustration of the singular value thresholding.

- As σ_{si} , σ_i , λ and $f'_\alpha(\sigma_{si})$ are non-negative, with respect to the equation (7) it is obvious that $\sigma_{si} \leq \sigma_i$.
- Since $\lim_{\sigma_{si} \rightarrow \infty} f'_\alpha(\sigma_{si}) = 0$, we obtain that the solution of the equation (7) is approximately equal to σ_i for the large singular values.
- Let $\lambda = \beta\alpha^2$, the derivative $\frac{\partial \sigma_{si}}{\partial \sigma_i}$ is equal to

$$\frac{\partial \sigma_{si}}{\partial \sigma_i} = \frac{1}{1 + 2\beta g(\sigma_{si}/\alpha)} = \frac{1}{J''_\beta(\sigma_{si}/\alpha)} \quad (8)$$

where $g(x) = \frac{1-3x^2}{(x^2+1)^3}$ and $J''_\beta(x) = 1 + 2\beta g(x)$. In the Appendix, it is proved that $J''_\beta(x) \geq 0$ for $\beta \leq 2$. Hence we can conclude that the singular value σ_{si} is an increasing function with respect to σ_i .

- Let $\lambda = 2\alpha^2$ ($\beta = 2$), if $\sigma_i = 2\alpha$, then it can be shown that with a simple calculation, the solution of the equation (7) is equal to $\sigma_{si} = \alpha$. As $g(1) = -1/4$, it is obvious that $\frac{\partial \sigma_{si}}{\partial \sigma_i} = +\infty$ for $\sigma_i = 2\alpha$.

Above properties illustrate obviously that the equation (7) is an operator of thresholding. Here we set the parameter λ to $2\alpha^2$. The reason of this selection is illustrated in the rest of this section. Fig. 2 shows the solution curve of $\sigma_{si} + 2\alpha^2 f'_\alpha(\sigma_{si}) = \sigma_i$ with respect to the variable σ_i for the different values of α . Here, we can see that the thresholding is softly done by the equation (7) with the threshold level of 2α . In the end of this section, we choose a suitable value of α with a heuristic view.

In order to define a new similarity measure, substituting (7) in the SSD term of $RRSSD_{LG}$ problem, we obtain $\|\mathbf{D}_T - \mathbf{S}\|_F^2 = \lambda^2 \sum_i f_\alpha'^2(\sigma_{si})$ with a simple calculation. Now, substituting this simplification in the $RRSSD_{LG}$ problem,

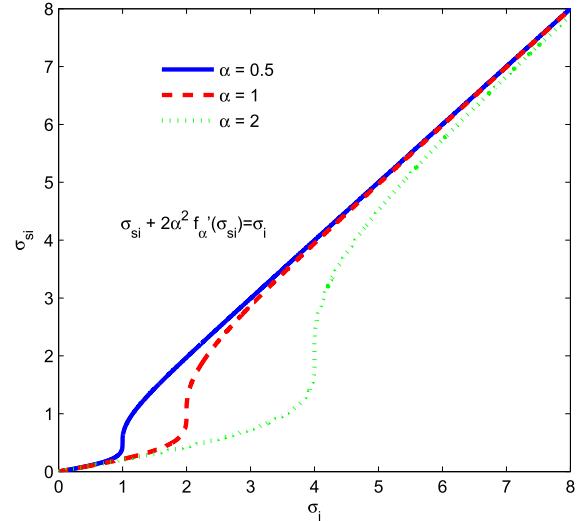


Fig. 2. The curve of $\sigma_{si} + 2\alpha^2 f'_\alpha(\sigma_{si}) = \sigma_i$ with respect to σ_i variable for different values of α .

we propose rank-regularized SSD (RRSSD) as a new similarity measure:

$$\begin{aligned} RRSSD(\mathbf{R}, \mathbf{F}) &= \sum_{i=1}^{\min(n,m)} f_\alpha(\sigma_{si}) + \frac{\lambda}{2} f_\alpha'^2(\sigma_{si}) \\ \mathbf{R} - \mathbf{F}(T) &= \mathbf{UDiag}\{\sigma_1, \dots, \sigma_{\min(n,m)}\}\mathbf{V}^T \\ \sigma_{si} + \lambda f'_\alpha(\sigma_{si}) &= \sigma_i, \quad i = 1, \dots, \min(n, m) \end{aligned} \quad (9)$$

Note that in this measure spatially varying intensity distortion \mathbf{S} is corrected analytically and its effect is present in the closed form of similarity measure via the singular value thresholding.

B. Parameter Selection

There are two parameters in our similarity measure: α and λ . With respect to the selection of $\lambda = 2\alpha^2$, one parameter must be determined. Here, we use two heuristic idea based on statistical view to chose these parameters as follows:

- To choose a suitable value of α , we consider the image registration problem only in the presence of Gaussian noise ($\mathbf{R} = \mathbf{F}(T) + \eta$). In this case, we expect that the SSD term is dominant in the $RRSSD_{LG}$ problem, and also the estimated \mathbf{S} is equal to zero matrix. To obtain these conditions, the thresholding level of 2α must be appropriately selected. From random matrix theory, it is known that if $\mathbf{Z} \in \mathbb{R}^{n \times n}$ is a random square matrix with i.i.d. entries and variance v_n^2 , $n^{-1/2} \|\mathbf{Z}\| \rightarrow \sqrt{2}v_n$, almost surely as $n \rightarrow \infty$, where $\|\mathbf{Z}\|$ is the largest singular value of \mathbf{Z} (the spectral norm) [30]. As $\mathbf{D}_T = \mathbf{R} - \mathbf{F}(T)$ is equal to the noise matrix $\eta \in \mathbb{R}^{n \times m}$ in the state of perfect registration, our proposal is $\alpha = \max\{\frac{\sqrt{n+m}}{2}v_n, 0.5\}$ with respect to the thresholding level 2α and the largest singular value of η ($\approx \sqrt{n+m}v_n$). With this selection, we expect that the estimated \mathbf{S} is approximately equal to zero matrix in the state of perfect registration, hence the SSD term is also dominant. As $\alpha \rightarrow 0$, $G_\alpha(\mathbf{S})$ is equal

to the rank of \mathbf{S} (ℓ_0 norm of singular values) which is not differentiable, we also consider the lower bound (0.5) for α .

- In this paper we set λ to $2\alpha^2 = \max\{\frac{n+m}{2}v_n^2, 0.5\}$. Here, we demonstrate that this selection appropriately quantifies trade-off between rank and SSD. On the other hand the two terms of SSD and rank have a same scale in the case of perfect registration. We know that the statistical expectation of $\|\mathbf{D}_T - \mathbf{S}\|_F^2$ is equal to $n m v_n^2$ in the state of perfect registration and the perfect correction of \mathbf{S} . Here we assume that the maximum value of $G_\alpha(\mathbf{S})$ is equal to $\min(n, m)/2$, i.e., $\text{rank}(\mathbf{S}) \leq \min(n, m)/2$. To have the same scale for the two terms of SSD and rank, the parameter λ is set to $\max(n, m)v_n^2$. We can see when the images are approximately square matrices ($n \approx m$), $2\alpha^2 \approx \max(n, m)v_n^2$. Hence, we observe that the selection of $\lambda = 2\alpha^2$ has a statistical view for quantifying trade-off between rank and SSD.

Here, the noise variance v_n^2 is also estimated from the wavelet coefficients of noisy image by the robust median estimator $v_n = \frac{\text{median}(|y_i|)}{0.6745}$, which is used from the finest scale wavelet coefficients ($y_i \in$ subband HH) [39].

C. Implementation

In this paper, Free Form Deformation (FFD) with three hierarchical levels of B-spline control points [40] is used as a model of geometric transform. Here, a transformation regularization is applied for smoothness of space warping. Let Θ be the displacements of B-spline control points which are the geometric transformation parameters, then inspired by [41], the new regularized similarity measure based on Laplacian approach is formulated as follows:

$$\hat{\Theta} = \underset{\Theta}{\operatorname{argmin}} \text{RRSSD}(R, F(T(\Theta))) + \frac{w}{2} \Theta^T \Lambda \Theta \quad (10)$$

where $\Lambda^{-1} = \mathbf{Q} \Delta \mathbf{Q}^T$, and $\Delta = \text{Diag}(k_i^2 |\mathbf{q}_i^T \Theta|^{-1})$ and $\mathbf{Q} = [\mathbf{q}_1, \dots, \mathbf{q}_N]$. The vector \mathbf{q}_i is the i^{th} basis of DCT, and $\{k_i\}_{i=1}^N$ are the eigenvalues of the discrete Laplacian on a regular grid [41]. The parameter w is the weight of the regularization term. The more details about this form of regularized problem (10) and its solution can be find in the literature [41]. The optimization process (10) is done iteratively to estimate the transform parameters using gradient descent. An important part of gradient computation is the gradient of RRSSD with respect to $\mathbf{D}_T = \mathbf{R} - \mathbf{F}(T)$. Inspired by [27], [29], this gradient is computed using the definition of sub-differential [42] with a simple calculation as follows:

$$\frac{\partial \text{RRSSD}(\mathbf{D}_T)}{\partial \mathbf{D}_T} = \text{UDiag}\{f'_\alpha(\sigma_{s1}), \dots, f'_\alpha(\sigma_{s \min(n,m)})\} \mathbf{V}^T. \quad (11)$$

The pseudo-code of image registration based on RRSSD is summarized in Algorithm 1.

III. EXPERIMENTAL RESULTS

The performance of our similarity measure is compared with SSD, MI, RC [22], SISM [11] and RISM [27] similarity measures. All approaches are implemented in Matlab, based on the

Algorithm 1 Non-Rigid Image Registration Based on RRSSD

- Initialization: Θ_0
 - For $j = 1, \dots, J$
 - Computing the similarity measure and its gradient:
 $\mathbf{D}_T = \mathbf{R} - \mathbf{F}(T(\Theta_{j-1}))$;
 $\text{SVD: } \mathbf{D}_T = \text{UDiag}\{\sigma_1, \dots, \sigma_{\min(n,m)}\} \mathbf{V}^T$;
 $\text{Thresholding: } \sigma_{si} + \lambda f'_\alpha(\sigma_{si}) = \sigma_i$;
 $\text{RRSSD}(\mathbf{R}, \mathbf{F}) = \sum_i f_\alpha(\sigma_{si}) + \frac{\lambda}{2} f'_\alpha(\sigma_{si})^2$;
 $\frac{\partial \text{RRSSD}(\mathbf{D}_T)}{\partial \mathbf{D}_T} = \text{UDiag}\{f'_\alpha(\sigma_{s1}), \dots, f'_\alpha(\sigma_{s \min(n,m)})\} \mathbf{V}^T$;
 $\nabla_\Theta \text{RRSSD} = -\frac{\partial \text{RRSSD}(\mathbf{D}_T)}{\partial \mathbf{D}_T} \nabla \mathbf{F}(T) \frac{\partial T}{\partial \Theta}$;
 $(\nabla \mathbf{F}$ is the intensity image gradient.)
 - Updating the transformation Θ :
 $\Theta_j = \mathbf{Q}(\mathbf{I} + \mu w \Delta)^{-1} \mathbf{Q}^T (\Theta_{j-1} - \mu \nabla_\Theta \text{RRSSD})$, (μ and \mathbf{I} are a small positive constant and the identity matrix, respectively);
-

Medical Image Registration Toolbox [22]. The experimental results have been performed on a personal computer with Intel Core i7 2.2GHz and 8GB RAM.

In this section, we evaluate the performance of the proposed non-rigid registration using the simulated database obtained from BrainWeb [43] and real data. The real data used are a clinically acquired computed tomography (CT) image data set, a video sequence of dynamic magnetic resonance imaging, a sequence of iris images, retina images, preoperative and intra-operative MRI images and digital subtraction angiography (DSA). Here, the robustness of the proposed similarity measure is also illustrated using its function with respect to the different geometric transform parameters.

A. Similarity Measure Functions

A similarity measure is an appropriate function to quantify the similarity between two images when its global minimum correctly represents the perfect alignment of two images. Fig. 3 presents the similarity measure functions of SSD, MI, RC, SISM, RISM and our method which are obtained between two images with respect to the different rotation and translation parameters. Obviously, RRSSD is a robust measure in the presence of illumination variations. The robustness of RC, SISM and RISM are also similar to RRSSD. We can see that SSD does not have an acceptable performance in the presence of spatially varying distortion, this result is also confirmed in the rest of this section. It seems that MI has a good distinguishable ability to represent the perfect registration. The reason of this result is the rigid transform in this example. If geometric transform is non-rigid, MI has a poor performance, which is shown in the simulated data.

B. Simulated Data: BrainWeb Images

In this experiment, the BrainWeb T1-weighted MRI images [43] are used. To evaluate the proposed similarity measure, we select a 2-D slice with size 216×180 . Here, the geometric transform is simulated by a FFD model that

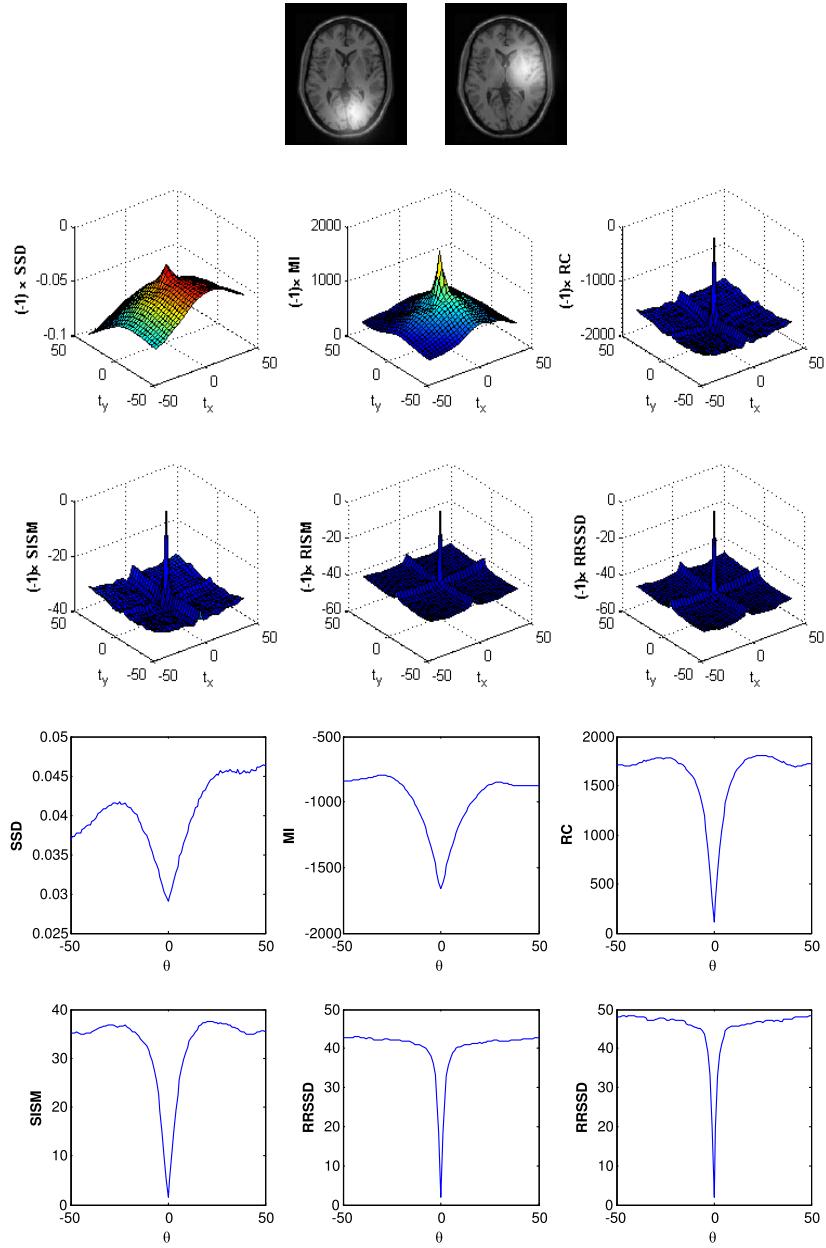


Fig. 3. Similarity measure functions of SSD, MI, RC, SISM, RISM and our approach in aligning the floating and reference images corrupted by spatially varying intensity distortion. Top row: the reference and floating images; The second and third rows: translation along the x and y axis; The fourth and fifth rows: rotation only.

its grid points are produced by perturbing a uniform grid of points. The grid size was 14×14 and its random perturbation was drawn from a uniform distribution on $[-6, 6]$ interval. The reference image is generated by applying this FFD transform.

To validate our similarity measure, the transformation root mean square error (RMSE) between the true and estimated transformations: $\varepsilon_{RMSE} = \sqrt{(1/N)\|T_{true} - T_{estimated}\|^2}$ is used. In all the experiments, mean and standard deviation (SD) of error measure are calculated by 20 runs of registration. The random intensity and spatially distortion were reinitialized at each run. In the rest of this subsection, the proposed approach is evaluated in the presence of four intensity distortions.

1) Experiment 1 (Additive Spatially Varying Intensity Distortion): Here, spatially varying intensity distortion of two images is modelled by additive bias field generated by the Gaussian functions as follows [11], [22], [25], [27]:

- $I(x, y) = I(x, y) + (1/K) \sum_{k=1}^K e^{-(\|x, y - \mu_k\|^2)/(2(30^2))}$
- rescale to $[0, 1]$.

The last term models locally varying intensity field with a mixture of K randomly centered Gaussian functions. **Fig. 4** shows one example of the registered images via different methods in the presence of spatially varying intensity distortion. It is obvious that SSD and MI have poor performance. We have highlighted the misalignment regions of these approaches with contours in **Fig. 4**. Other methods

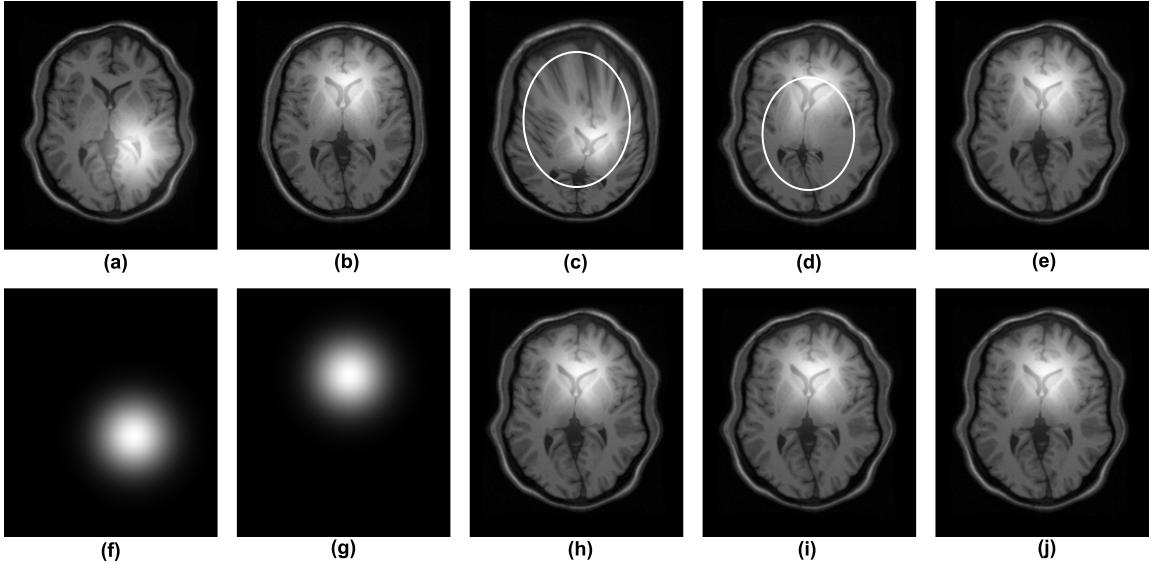


Fig. 4. We register the floating image (b) onto the reference image (a) in the presence of intensity distortion field. (a) Reference image. (b) floating image. (c) SSD result. (d) MI result. (e) RC result. (f) Reference bias. (g) floating bias. (h) SISM result. (i) RISM result. (j) RRSSD result.

TABLE I

REGISTRATION PERFORMANCES OF RRSSD, RISM, SISM, RC, SSD AND MI. BOTH IMAGES WERE CORRUPTED BY BIAS FIELD

Transformation RMSE(SD)						
K	Additive Distortion			Multiplicative Distortion		
	1	3	5	1	3	5
MI	10.1314 (6.2347)	5.4932 (2.7287)	3.5808 (1.8439)	4.3637 (3.4683)	2.2422 (0.5177)	2.2071 (0.6752)
SSD	19.4352 (12.8823)	6.5821 (4.4376)	3.1735 (1.2430)	11.2105 (6.7694)	6.1284 (4.4593)	2.7612 (1.3197)
RC	1.0507 (0.1303)	0.8690 (0.1108)	0.8378 (0.1028)	1.2431 (0.2128)	1.0374 (0.2740)	0.8671 (0.2131)
SISM	1.0571 (0.0751)	0.8140 (0.1861)	0.7763 (0.1209)	1.3314 (0.2414)	0.9489 (0.2512)	0.8010 (0.2020)
RISM	0.7768 (0.1217)	0.7789 (0.2296)	0.7282 (0.1818)	1.1447 (0.3613)	0.9612 (0.3037)	0.8513 (0.3122)
RRSSD	0.7653 (0.0810)	0.7446 (0.1955)	0.6757 (0.1907)	1.0438 (0.4472)	0.9081 (0.3800)	0.8888 (0.3948)

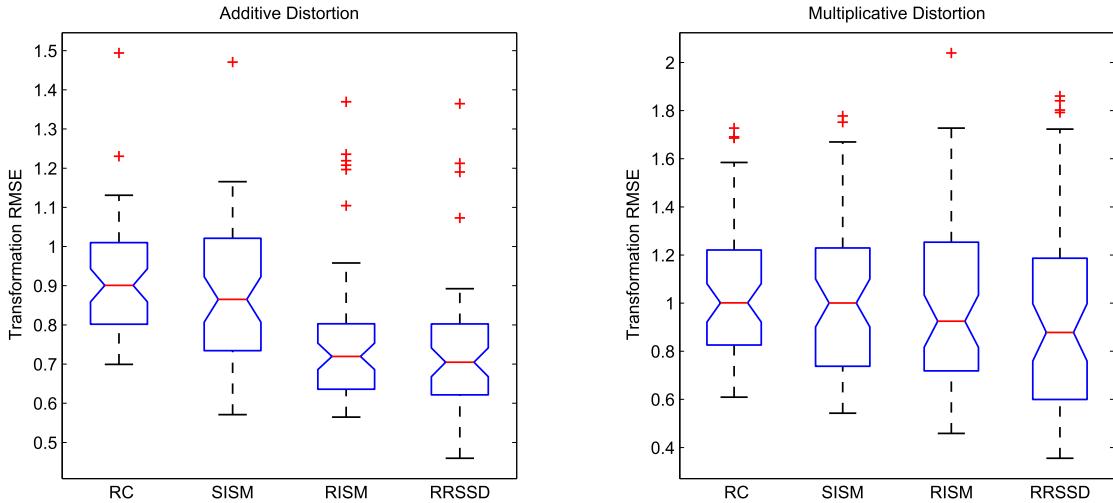


Fig. 5. Registration performances of RRSSD, RISM, SISM, RC. Both images were corrupted by bias field. Box-plot representation of the error distributions is shown for all similarity measures. On each box, the central line is the median, the edges of the box are the 25th and 75th percentiles, the whiskers extend to the most extreme data points not considered outliers. Red crosses represent outliers outside 1.5 times the interquartile range. The value of 1.5 corresponds to approximately $\pm 2.7\sigma$ and 99.3 coverage if the data are normally distributed.

have acceptable performance. We can see that RRSSD which is a modified SSD, has an accurate performance.

Table I shows the registration performance of all similarity measures for the different values of K . For the cumulative validation of 60 runs (all 20 runs for each K), the mean

(standard deviation) registration errors were 9.7303 (8.7352), 6.4018 (4.8686), 0.9192 (0.1476), 0.8825 (0.1828), 0.7613 (0.1815) and 0.7286 (0.1662) for the SSD, MI, RC, SISM, RISM and RRSSD measures, respectively. Here, Fig. 5 visualizes the registration performance of different approaches

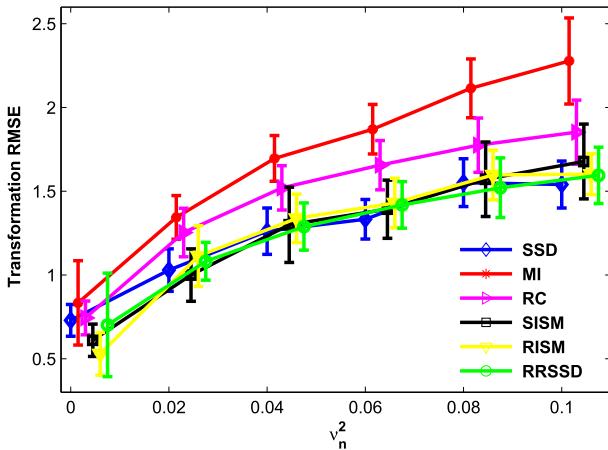


Fig. 6. Registration performances of RRSSD, RISM, SISM, RC, SSD, and MI. Floating image was corrupted by the Gaussian noise.

as the box-plot representation which shows the distribution of registration error. We can see that the RRSSD outperforms other state-of-the-art measures such as the effective measures of RC, SISM and RISM. Also the proposed measure has sub-pixel and clinically acceptable accuracy.

Here, the criteria of computation time is used to compare the computational complexity of different approaches. RRSSD, RISM, SISM and RC have approximately the same average computation time which was 40 seconds for the registration of a pair of images. Traditional similarity measures of MI and SSD are not robust in the presence of spatially varying intensity distortion, hence, comparing the computational complexity of RRSSD and these methods is meaningless.

2) Experiment 2 (Multiplicative Spatially Varying Intensity Distortion): In this experiment, to evaluate the proposed approach, we use the multiplicative distortion using the following formula.

$$I(x, y) = I(x, y) \cdot (0.5 + (1/K) \sum_{k=1}^K e^{-(\|x, y\| - \mu_k\|^2)/(2(30^2))})$$

The results of this evaluation are shown in [Table I](#). It can be seen that the proposed approach outperforms other similarity measures. For the cumulative validation of 60 runs (all 20 runs for each K), the mean (standard deviation) registration errors were 9.7303 (8.7352), 2.9377 (2.2674), 1.0492 (0.2782), 1.0271 (0.3210), 0.9858 (0.3436) and 0.9469 (0.4073) for the SSD, MI, RC, SISM, RISM and RRSSD measures, respectively. The box-plot representation of the registration results is also shown for RC, SISM, RISM and RRSSD similarity measures in [Fig. 5](#). It is clear that RRSSD has a better performance with sub-pixel accuracy.

3) Experiment 3 (Additive Gaussian Noise): Here, we evaluate the proposed approach in the presence of stationary intensity distortion of Gaussian noise. Floating image is corrupted by additive zero mean Gaussian noise. The registration accuracy results of all approaches are shown in [Fig. 6](#). A importance note about these results is that the methods of SSD, SISM, RISM and RRSSD have similar performances. This note can be illustrated as three sparse

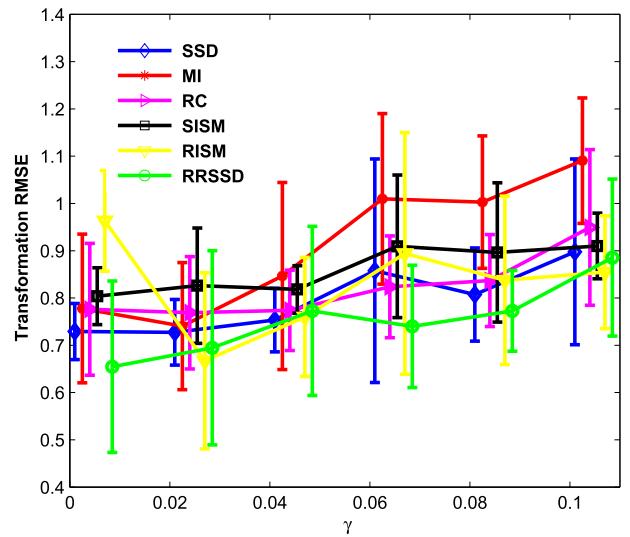


Fig. 7. Registration performances of RRSSD, RISM, SISM, RC, SSD, and MI. Floating image was corrupted by the Laplace noise.

(sparsity in the transform domain or singular value domain) based similarity measures (SISM, RISM and RRSSD) are equivalent to the SSD measure in the presence of Gaussian noise [11], [27]. As SSD is an optimal measure in the presence of this distortion, and RRSSD is a generalized form of SSD, we expect that RRSSD has a better performance in the presence of this distortion. The results also confirm this evidence.

4) Experiment 4 (Laplace Noise): In this experiment, the additive intensity distortion is assumed to be the zero mean Laplace noise $1/2\gamma \exp(|x|/\gamma)$. [Fig. 7](#) shows the registration performance versus the parameter γ . This noise is non-Gaussian, which is not considered in the definition of the proposed similarity measure. This experiment shows that the proposed approach has better registration accuracy in the presence of this distortion.

5) Sensitivity Analysis: Here, we study the sensitivity of our approach with respect to varying the parameter α . The proposed similarity measure has only one parameter α , which is proposed to be set to $\alpha = \max\{\frac{\sqrt{n+m}}{2}v_n, 0.5\}$ where v_n^2 is the variance of noise. We conduct 20 runs of image registration in the presence of additive spatially varying intensity distortion ($K = 3$) and stationary intensity distortion of Gaussian noise for each value of α in the interval $[0.5, 3]$. [Fig. 8](#) shows the registration accuracy results obtained for various α . Here, the proposed approach is evaluated for two different values of noise variance $v_n^2 = 0.01$ and $v_n^2 = 0.04$. The proposed parameters α using the mentioned formula for these variances are 1 and 2, respectively. As [Fig. 8](#) shows, the proposed formula is an appropriate choice for the parameter α and the these selected α parameters are approximately the global minimum of the presented evaluation curves. We can see that the registration accuracy is not sensitive to varying the α parameter close to the proposed one.

C. The registration of Inhale and Exhale CT Scans

Here, to evaluate the proposed similarity measure, we perform non-rigid registration on four CT scan pairs,

TABLE II

DESCRIPTION OF CLINICAL CASES AND 3-D VOLUME REGISTRATION ACCURACY: THE MEAN AND STANDARD DEVIATION OF 3-D REGISTRATION ERRORS. HERE DISPLACEMENT INDICATES THE 3D DISTANCE BETWEEN EACH PAIR OF LANDMARKS IN THE MAXIMUM EXHALE AND INHALE IMAGES, AND SD REPRESENTS STANDARD DEVIATION

case	Displacement mean (SD) (mm)	Image dimension	Voxel size (mm)	Displacement mean (SD) (mm) after registration					
				SSD	MI	RC	SISM	RISM	RRSSD
1	3.8924 (2.7839)	256 × 256 × 94	0.97 × 0.97 × 2.5	1.0501 (0.5370)	1.2110 (0.6285)	1.1880 (0.7185)	1.0296 (0.4898)	1.0323 (0.5364)	1.0261 (0.5193)
2	4.3378 (3.9016)	256 × 256 × 112	1.16 × 1.16 × 2.5	1.2615 (1.0284)	1.7013 (1.6513)	1.3387 (1.1315)	1.2362 (0.9734)	1.1887 (0.8586)	1.1864 (0.8732)
3	6.9430 (4.0519)	256 × 256 × 104	1.15 × 1.15 × 2.5	1.7402 (1.7639)	2.7229 (2.3208)	1.9392 (2.0834)	1.7074 (1.6008)	1.7728 (1.5231)	1.6973 (1.3968)
4	9.8301 (4.8604)	256 × 256 × 99	1.13 × 1.13 × 2.5	1.7046 (1.5712)	2.2194 (1.9719)	1.6949 (1.5955)	1.6107 (1.3863)	1.6643 (1.4947)	1.6001 (1.4103)

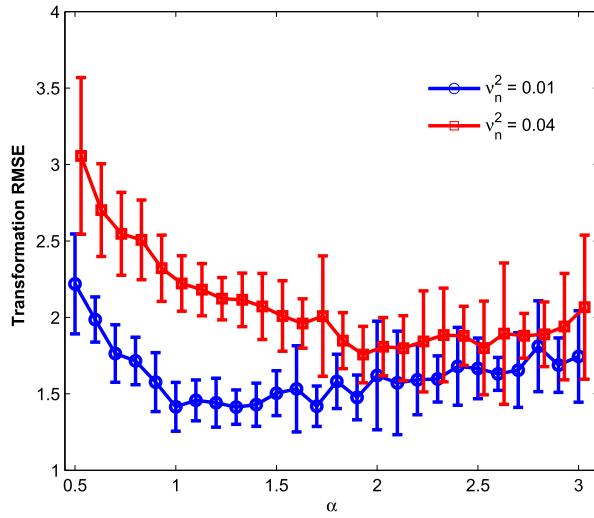


Fig. 8. Registration performance of RRSSD with respect to the different parameter α settings.

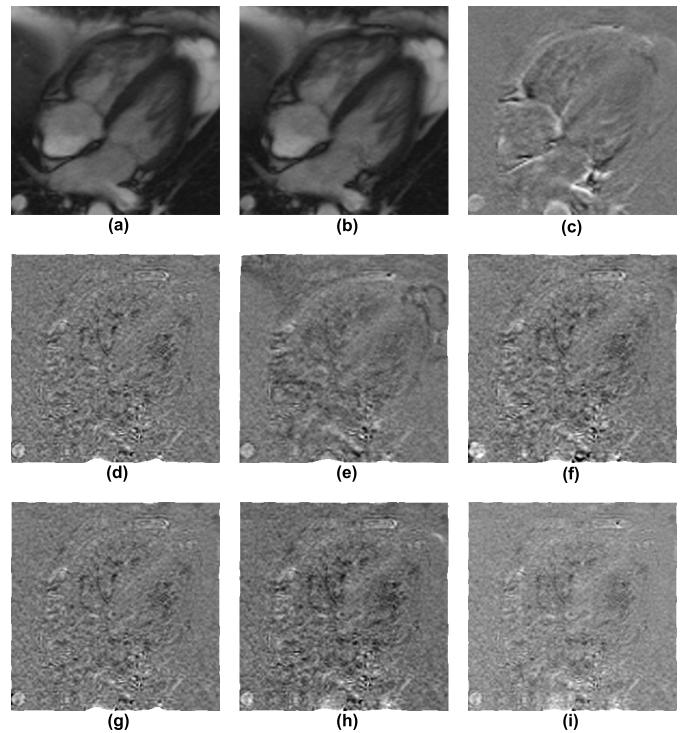


Fig. 10. Dynamic cardiac MRI: (a) Reference (frame 3). (b) Floating (frame 4). (c) Difference image before registration. Difference images after registration using (d) SSD, (e) MI, (f) RC, (g) SISM, (h) RISM and (i) RRSSD.

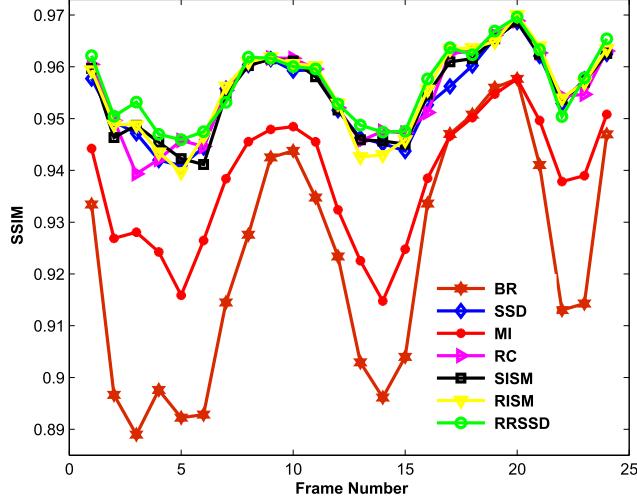


Fig. 9. Registration accuracy: frame by frame of dynamic cardiac MRI are registered to estimate the motion of cardiac through time. Here, The BR curve shows the SSIM before registration (BR).

maximum inhale (floating image) and maximum exhale (reference image) of a breathing cycle provided by the DIR-Lab at the University of Texas [44]. In this data, patients

were treated for esophagus cancer. In each image, 300 anatomical landmarks as ground truth of image registration have been carefully annotated by thoracic imaging experts. Properties of CT data such as size and resolution are shown in Table II. As the proposed similarity measure of RRSSD is defined between two matrices, we use the similarity measure between all 2D slices of 3D data to implement the proposed measure on 3D data.

To quantify the registration accuracy, the manually extracted landmarks per scan pair are used. The average target registration error for the expert landmark and the corresponding standard deviations for each method on each case are shown in Table II. It is obvious that our method achieved lower registration errors than those of RISM, SISM, RC, SSD, and MI. For the cumulative validation of 1200 landmark pairs

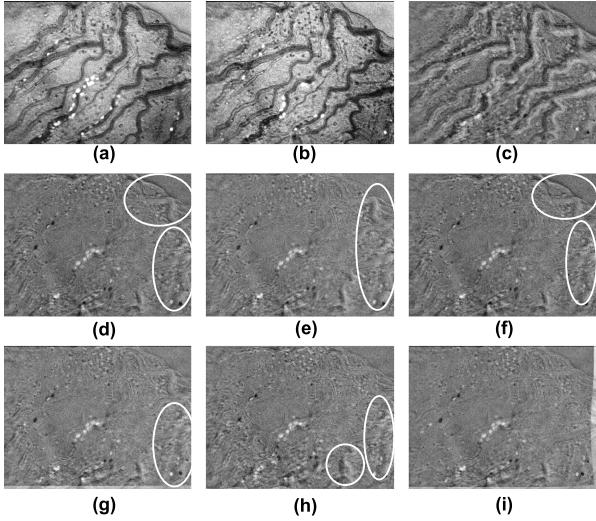


Fig. 11. Iris images: (a) Reference (frame 1). (b) floating (frame 19). (c) Difference image before registration. Difference images after registration using (d) SSD, (e) MI, (f) RC, (g) SISM, (h) RISM and (i) RRSSD.

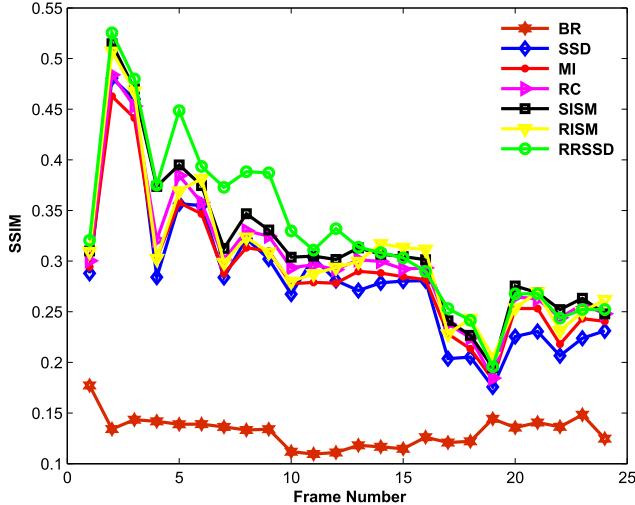


Fig. 12. Registration accuracy: frame by frame of iris video sequence are registered. Here, The BR curve shows the SSIM before registration (BR).

(all 300 landmarks for all 4 cases), the average (standard deviation) registration errors were 1.3775 (1.1480), 1.4145 (1.2200), 1.3960 (1.1126), 1.5402 (1.3822), 1.4391 (1.2251), and 1.9636 (1.6431) for the proposed method, RISM, SISM, RC, SSD, and MI, respectively.

D. Dynamic Cardiac MRI

An important application of image registration is the analysis of heart motion for investigating the heart's architecture and function [45]. Here, we register two consecutive frames of a sequence of 2D dynamic cardiac MRI through time to evaluate the proposed measure. The Dynamic MRI sequence was acquired using a Siemens Avanto 1.5T at Rajaei hospital, Tehran, Iran. Fig. 9 shows the registration accuracy via the structural similarity (SSIM) index [46] versus the frame number. It is obvious that RRSSD has better performance. We also visually evaluated all approaches using the difference image

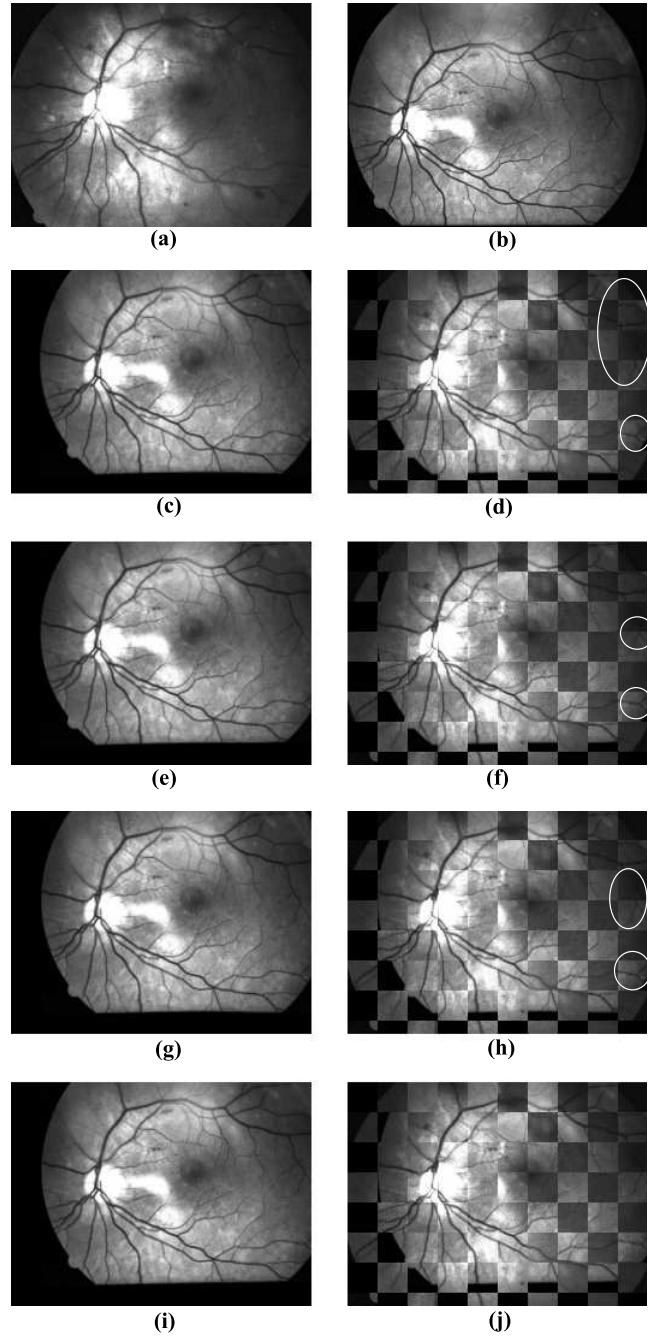


Fig. 13. Registration of retina images: (a) reference image. (b) source image. (c) RC result. (d) composite view of RC result. (e) SISM result. (f) composite view of SISM result. (g) RISM result. (h) composite view of RISM result. (i) RRSSD result. (j) composite view of RRSSD result.

after registration on a pair of image frames in Fig. 10. It can be seen that the RRSSD difference image has the most uniform texture. Thus the proposed method has a good performance for estimating the heart motion.

E. Iris Images

Image registration is an important pre-process in the application of tracking leukocytes to study immune systems. A sequence of iris images is useful for this application [47], [32]. In this problem, motion estimation suffers

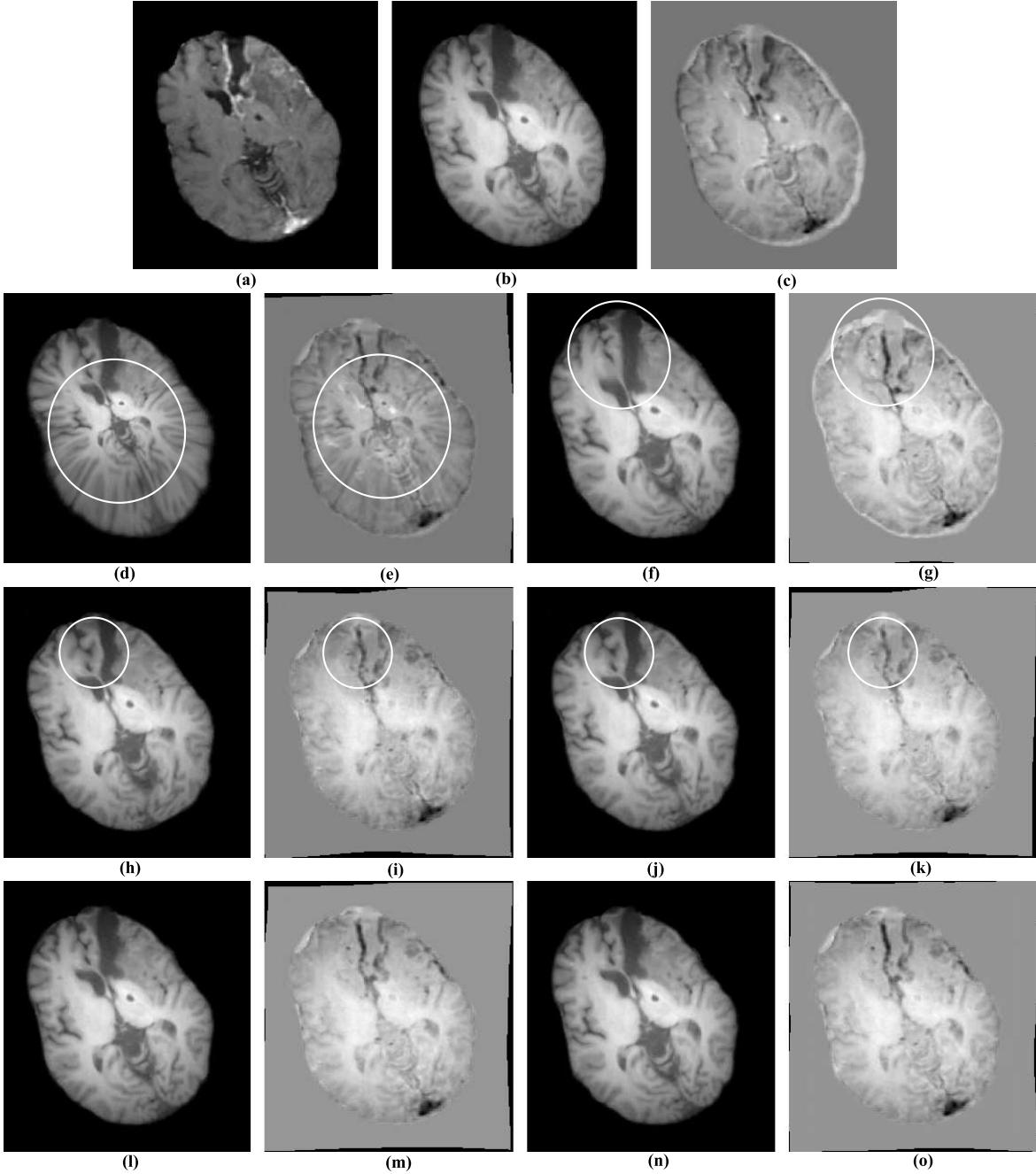


Fig. 14. Registration of the preoperative and intra-operative MRI images: (a) reference image (intra-operative MRI). (b) source image (preoperative MRI). (c) Difference image before registration. (d) SSD result. (e) Difference image after SSD result. (f) MI result. (g) Difference image after MI result. (h) RC result. (i) Difference image after RC result. (j) SISM result. (k) Difference image after SISM result. (l) RISM result. (m) Difference image after RISM result. (n) RRSSD result. (o) Difference image after RRSSD result.

from the presence of spatially varying intensity distortion. Here, to evaluate the proposed approach, we stabilized and rectified a microscopic iris video sequence consisting of 25 frames with registering each frame onto the first frame. Fig. 11 presents an example of the registration result on a pair of image frames using the difference image after registration. Also, this example shows the presence of spatially varying intensity distortion. In this figure, we have highlighted the misalignment regions of other approaches with contours. It is seen that the motion artifacts are significantly reduced using

the proposed approach. Fig. 12 shows the registration accuracy via the SSIM index [46] versus the frame number. It is obvious that RRSSD has better accuracy.

F. Retina Images

Another application of image registration is in the retina images taken two years apart [48]. These images are useful in ophthalmology. These images are affected by the presence of spatially varying intensity distortion because of

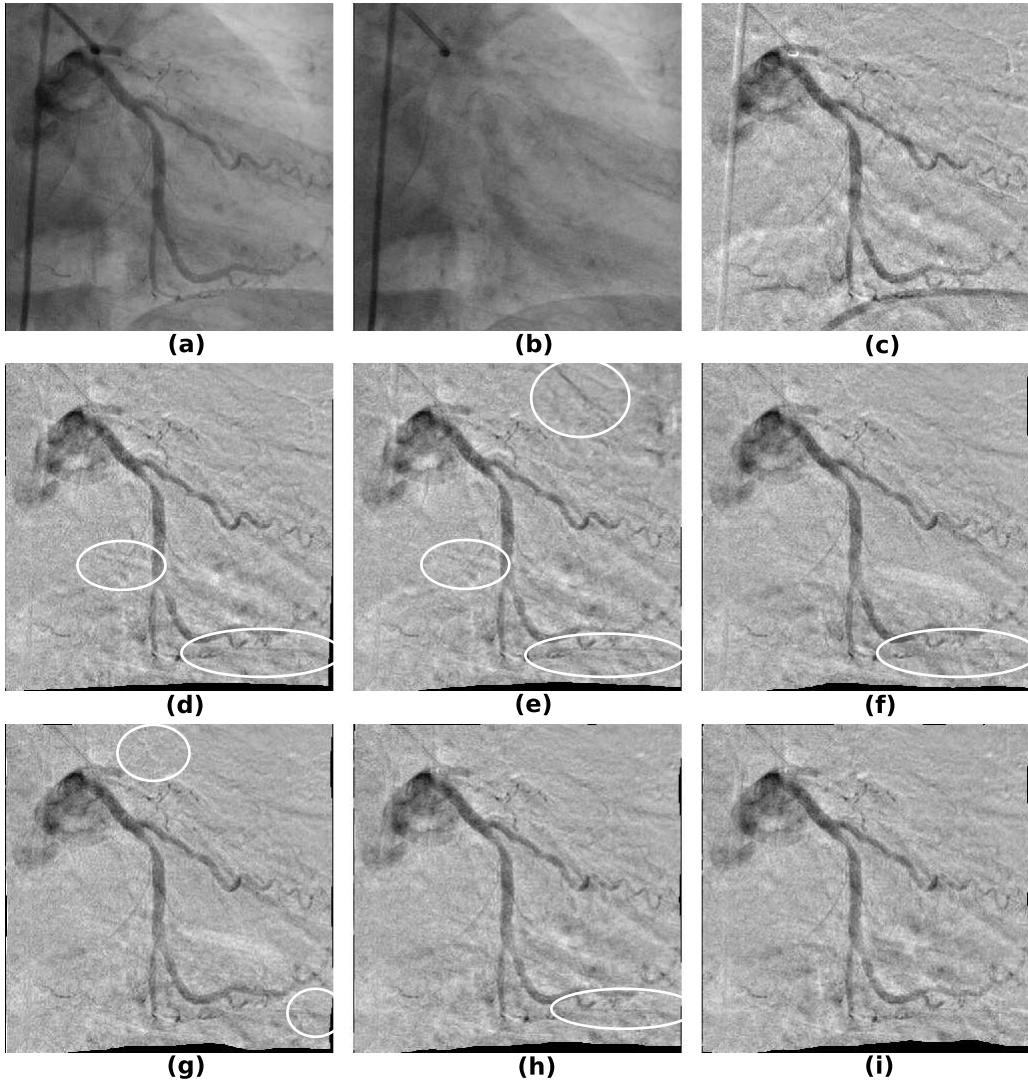


Fig. 15. Registration of coronary angiographic images. (a) Image after the injection of the contrast agent; (b) Image before the injection of the contrast agent. (c) DSA image before registration. DSA images after the motion compensation using (d) SSD, (e) MI, (f) RC, (g) SISM, (h) RISM and (i) RRSSD.

non-uniform background and blood vessels (Fig. 13). Hence the feature based methods have the main role for solving this challenge [49].

Intensity methods such as SSD and MI have very poor performance in this application. In this paper, we show that the regularized SSD based on the low rank matrix theory is an appropriate measure for this application. Fig. 13 demonstrates the registration results. The proposed measure has accurate registration performance as demonstrated via composite view. We can see from composite view that RC, SISM and RISM have some misalignments in low-contrast regions. In Fig. 13, we have highlighted the misalignment regions with contours.

G. Real Images of Preoperative MRI and Intra-Operative MRI

In order to evaluate the proposed approach, we register the preoperative MRI and the intra-operative MRI images (Fig. 14) which are captured for measuring tumor resection surgery [50]. The main challenge of this registration problem is the role of

tumor image as outlier data. In this paper, the low rank matrix has been used to model the outlier data. The tumor image can be modelled by a low rank matrix, so the proposed approach has clinically acceptable accuracy in this problem.

Fig. 14 presents the registration results of all similarity measures. SSD and MI have poor performance in the presence of outlier data. We have highlighted the misalignment regions with contours in Fig. 14. It is obvious that the proposed approach compensates the motion artefacts significantly in the presence of tumor.

H. Digital Subtraction Angiography

Digital subtraction angiography (DSA) is a type of imaging technique used to clearly visualize blood vessels in the human body [51]. In this approach, a sequence of images is taken during the injection of contrast agent through vessels of interest. To highlight and visualise blood vessels, the subtraction of two images which are taken before and after the injection of contrast agent is used to remove the background effects.

Before the subtraction process, some movements such as breath and patient movements must be compensated. Image registration is a main preprocessing task to obtain DSA images. The significant challenge of this problem is the slow varying-intensity distortions as a result of contrast agent enhancement. Fig. 15 presents two real DSA images and the results of different methods. In this figure, we have highlighted the misalignment regions with contours. It can be seen that the proposed approach has better registration performance.

IV. DISCUSSION AND CONCLUSION

In this paper, we proposed the low rank matrix to model spatially varying intensity distortion in image registration application. Based on this model, we derived a new similarity measure based on the low rank theory. This measure is a modified version of SSD based on the low rank matrix regularization. SSD is not an appropriate similarity measure in the presence of spatially varying distortion because of pixel by pixel dependency of this distortion. In this paper, we combine the SSD measure with the sparse representation of this distortion in the singular value domain. The SSD term considers the Gaussian noise and the sparsity measure consider the spatially varying intensity distortion. The important property of RRSSD is that this distortion is estimated analytically and compensated in the SSD term. This is the main difference of the proposed similarity measure with SISM and RISM which are sparse measures in the different domains of transform and singular value, respectively. We experimentally showed that our proposed measure outperforms other state-of-the-art similarity measures in real and simulated data.

Our similarity measure has an advantage of simplicity in terms of computational complexity and implementation. The proposed measure contains three steps: singular value decomposition of difference image, singular value thresholding and RRSSD calculation. Computation time needed for registration of a pair of images is similar to other similarity measures.

The measure of RRSSD has only one parameter α which is computed via the estimation of noise variance. Our sensitivity analysis test shown that the registration performance is not sensitive to the small error of estimated α .

Future work will focus on extending our approach to multi-modal image registration and considering the multiplicative distortion analytically.

APPENDIX THE PROOF OF LEMMA 1

It is obvious that $J_{\lambda,\alpha}(x) = \frac{1}{2}(x - a)^2 + \lambda \frac{x^2}{x^2 + \alpha^2}$ is twice continuously differentiable and its domain is the real line, hence this function is convex if and only if $J''_{\lambda,\alpha}(x) \geq 0$ for all x . To prove the convexity the following notes are helpful to simplify the proof:

- With respect to the function $(x - a)^2$ and the convexity condition ($J''_{\lambda,\alpha}(x) \geq 0$), it is obvious that the parameter "a" don't have any role in this condition. Hence in the rest of the proof we set this to zero.
- Let $\lambda = \beta\alpha^2$ where $\beta \geq 0$, with this selection after some calculations we can conclude that the parameter α has

the role of scaling in the function $J_{\lambda,\alpha}(x)$, hence this parameter don't limit the convexity condition.

With respect to the above notes, it is sufficient to prove the convexity condition of the following function:

$$J_\beta(x) = \frac{1}{2}x^2 + \beta \frac{x^2}{x^2 + 1} \quad (12)$$

The second derivative $J''_\beta(x)$ is equal to

$$J''_\beta(x) = 1 + 2\beta g(x) \quad (13)$$

where $g(x) = \frac{1-3x^2}{(x^2+1)^3}$. It can be shown that $g(x) \geq g(1) = -1/4$. With respect to this property, it is observable that the convexity condition ($J''_\beta(x) \geq 0$) is equivalent to $\beta \leq 2$ and the proof is completed.

REFERENCES

- A. Sotiras, C. Davatzikos, and N. Paragios, "Deformable medical image registration: A survey," *IEEE Trans. Med. Imag.*, vol. 32, no. 7, pp. 1153–1190, Jul. 2013.
- J. Ma, J. Zhao, and J. Tian, "Nonrigid image deformation using moving regularized least squares," *IEEE Signal Process. Lett.*, vol. 20, no. 10, pp. 988–991, Oct. 2013.
- J. Ma, W. Qiu, J. Zhao, Y. Ma, A. L. Yuille, and Z. Tu, "Robust $L_2 E$ estimation of transformation for non-rigid registration," *IEEE Trans. Signal Process.*, vol. 63, no. 5, pp. 1115–1129, Mar. 2015.
- J. Ma, J. Zhao, J. Tian, A. L. Yuille, and Z. Tu, "Robust point matching via vector field consensus," *IEEE Trans. Image Process.*, vol. 23, no. 4, pp. 1706–1721, Apr. 2014.
- J. Ma, Y. Ma, J. Zhao, and J. Tian, "Image feature matching via progressive vector field consensus," *IEEE Signal Process. Lett.*, vol. 22, no. 6, pp. 767–771, Jun. 2015.
- H. Zhou and H. Rivaz, "Registration of pre- and postresection ultrasound volumes with noncorresponding regions in neurosurgery," *IEEE J. Biomed. Health Inform.*, vol. 20, no. 5, pp. 1240–1249, Sep. 2016.
- A. Roche, G. Malandain, X. Pennec, and N. Ayache, "The correlation ratio as a new similarity measure for multimodal image registration," in *Medical Image Computing and Computer-Assisted Intervention* (Lecture Notes in Computer Science), vol. 1496. Berlin, Germany: Springer-Verlag, 1998, pp. 1115–1124.
- W. M. Wells, P. Viola, H. Atsumi, S. Nakajima, and R. Kikinis, "Multi-modal volume registration by maximization of mutual information," *Med. Image Anal.*, vol. 1, no. 1, pp. 35–51, 1996.
- H. Rivaz, Z. Karimaghloo, and D. L. Collins, "Self-similarity weighted mutual information: A new nonrigid image registration metric," *Med. Image Anal.*, vol. 18, no. 2, pp. 343–358, 2014.
- H. Rivaz, Z. Karimaghloo, V. S. Fonov, and D. L. Collins, "Nonrigid registration of ultrasound and MRI using contextual conditioned mutual information," *IEEE Trans. Med. Imag.*, vol. 33, no. 3, pp. 708–725, Mar. 2014.
- A. Ghaffari and E. Fatemizadeh, "Sparse-induced similarity measure: Mono-modal image registration via sparse-induced similarity measure," *IET Image Process.*, vol. 8, no. 12, pp. 728–741, 2014.
- M. F. Azampour, A. Ghaffari, A. Hamidinekoo, and E. Fatemizadeh, "Manifold learning based registration algorithms applied to multi-modal images," in *Proc. 36th Annu. Int. Conf. IEEE Eng. Med. Biol. Soc. (EMBC)*, Sep. 2014, pp. 1030–1034.
- C. Wachinger and N. Navab, "Manifold learning for multi-modal image registration," in *Proc. BMVC*, 2010, pp. 1–12.
- C. Wachinger and N. Navab, "Entropy and laplacian images: Structural representations for multi-modal registration," *Med. Image Anal.*, vol. 16, no. 1, pp. 1–17, 2012.
- M. M. Fouad, R. M. Dansereau, and A. D. Whitehead, "Image registration under illumination variations using region-based confidence weighted M-estimators," *IEEE Trans. Image Process.*, vol. 21, no. 3, pp. 1046–1060, Mar. 2012.
- A. Roche, G. Malandain, and N. Ayache, "Unifying maximum likelihood approaches in medical image registration," *Int. J. Imag. Syst. Technol.*, vol. 11, no. 1, pp. 71–80, 2000.
- P. P. Wyatt and J. A. Noble, "MAP MRF joint segmentation and registration of medical images," *Med. Image Anal.*, vol. 7, no. 4, pp. 539–552, 2003.

- [18] C. Studholme, C. Drapaca, B. Iordanova, and V. Cardenas, "Deformation-based mapping of volume change from serial brain MRI in the presence of local tissue contrast change," *IEEE Trans. Med. Imag.*, vol. 25, no. 5, pp. 626–639, May 2006.
- [19] D. Loeckx, P. Slagmolen, F. Maes, D. Vandermeulen, and P. Suetens, "Nonrigid image registration using conditional mutual information," *IEEE Trans. Med. Imag.*, vol. 29, no. 1, pp. 19–29, Jan. 2010.
- [20] L. Wang and C. Pan, "Nonrigid medical image registration with locally linear reconstruction," *Neurocomputing*, vol. 145, pp. 303–315, Dec. 2014.
- [21] K. Aghajani, M. T. Manzuri, and R. Yousefpour, "A robust image registration method based on total variation regularization under complex illumination changes," *Comput. Meth. Progr. Biomed.*, vol. 134, pp. 89–107, Jun. 2016.
- [22] A. Myronenko and X. Song, "Intensity-based image registration by minimizing residual complexity," *IEEE Trans. Med. Imag.*, vol. 29, no. 11, pp. 1882–1891, Nov. 2010.
- [23] P. Farnia, A. Ahmadian, T. Shabani, N. D. Serej, and J. Alirezaie, "Brain-shift compensation by non-rigid registration of intra-operative ultrasound images with preoperative mr images based on residual complexity," *Int. J. Comput. Assist. Radiol. Surg.*, vol. 10, no. 5, pp. 555–562, 2014.
- [24] K. Aghajani, R. Yousefpour, M. Shirpour, and M. T. Manzuri, "Intensity based image registration by minimizing the complexity of weighted subtraction under illumination changes," *Biomed. Signal Process. Control*, vol. 25, pp. 35–45, Mar. 2016.
- [25] A. Ghaffari and E. Fatemizadeh, "Robust Huber similarity measure for image registration in the presence of spatially-varying intensity distortion," *Signal Process.*, vol. 109, pp. 54–68, Apr. 2015.
- [26] M. Afzali, A. Ghaffari, E. Fatemizadeh, and H. Soltanian-Zadeh, "Medical image registration using sparse coding of image patches," *Comput. Biol. Med.*, vol. 73, pp. 56–70, Jun. 2016.
- [27] A. Ghaffari and E. Fatemizadeh, "RISM: Single-modal image registration via rank-induced similarity measure," *IEEE Trans. Image Process.*, vol. 24, no. 12, pp. 5567–5580, Dec. 2015.
- [28] K. Konstantinides and K. Yao, "Statistical analysis of effective singular values in matrix rank determination," *IEEE Trans. Acoust., Speech, Signal Process.*, vol. ASSP-36, no. 5, pp. 757–763, May 1988.
- [29] M. Malek-Mohammadi, M. Babaie-Zadeh, A. Amini, and C. Jutten, "Recovery of low-rank matrices under affine constraints via a smoothed rank function," *IEEE Trans. Signal Process.*, vol. 62, no. 4, pp. 981–992, Feb. 2014.
- [30] E. J. Candès and Y. Plan, "Matrix completion with noise," *Proc. IEEE*, vol. 98, no. 6, pp. 925–936, Jun. 2010.
- [31] B. Recht, M. Fazel, and P. A. Parrilo, "Guaranteed minimum-rank solutions of linear matrix equations via nuclear norm minimization," *SIAM Rev.*, vol. 52, no. 3, pp. 471–501, 2010.
- [32] Y. Peng, A. Ganesh, J. Wright, W. Xu, and Y. Ma, "RASL: Robust alignment by sparse and low-rank decomposition for linearly correlated images," *IEEE Trans. Pattern Anal. Mach. Intell.*, vol. 34, no. 11, pp. 2233–2246, Nov. 2012.
- [33] V. Hamy *et al.*, "Respiratory motion correction in dynamic MRI using robust data decomposition registration—Application to DCE-MRI," *Med. Image Anal.*, vol. 18, no. 2, pp. 301–313, 2014.
- [34] J. Wright, A. Ganesh, S. Rao, Y. Peng, and Y. Ma, "Robust principal component analysis: Exact recovery of corrupted low-rank matrices via convex optimization," in *Proc. Neural Inf. Process. Syst. (NIPS)*, 2009, pp. 2080–2088.
- [35] E. J. Candès, X. Li, Y. Ma, and J. Wright, "Robust principal component analysis?" *J. ACM*, vol. 58, no. 3, p. 11, May 2011.
- [36] Z. Zhang, A. Ganesh, X. Liang, and Y. Ma, "TILT: Transform invariant low-rank textures," *Int. J. Comput. Vis.*, vol. 99, no. 1, pp. 1–24, 2012.
- [37] M. Fazel, "Matrix rank minimization with applications." Ph.D. dissertation, Dept. Elect. Eng., Stanford Univ., Stanford, CA, USA, 2002.
- [38] H. Zhou and L. Li, "Regularized matrix regression," *J. Roy. Statist. Soc. B (Statist. Methodol.)*, vol. 76, no. 2, pp. 463–483, 2014.
- [39] D. L. Donoho and J. M. Johnstone, "Ideal spatial adaptation by wavelet shrinkage," *Biometrika*, vol. 81, no. 3, pp. 425–455, 1994.
- [40] D. Rueckert, L. I. Sonoda, C. Hayes, D. L. G. Hill, M. O. Leach, and D. J. Hawkes, "Nonrigid registration using free-form deformations: Application to breast MR images," *IEEE Trans. Med. Imag.*, vol. 18, no. 8, pp. 712–721, Aug. 1999.
- [41] A. Myronenko and X. Song, "Adaptive regularization of ill-posed problems: Application to non-rigid image registration," *CoRR*, vol. 6, pp. 1–10, Jun. 2009.
- [42] A. S. Lewis, "The convex analysis of unitarily invariant matrix functions," *J. Convex Anal.*, vol. 2, no. 1, pp. 173–183, 1995.
- [43] C. A. Cocosco, V. Kollokian, R. K.-S. Kwan, and A. C. Evans, "BrainWeb: Online interface to a 3D MRI simulated brain database," *NeuroImage*, vol. 5, no. 4, p. S425, 1997. [Online]. Available: <http://www.bic.mni.mcgill.ca/brainweb/>
- [44] R. Castillo *et al.*, "A framework for evaluation of deformable image registration spatial accuracy using large landmark point sets," *Phys. Med. Biol.*, vol. 54, no. 7, pp. 1849–1870, 2009. [Online]. Available: <http://www.dir.lab.com>
- [45] X. Papademetris, A. J. Sinusas, D. P. Dione, R. T. Constable, and J. S. Duncan, "Estimation of 3D left ventricular deformation from medical images using biomechanical models," *IEEE Trans. Med. Imag.*, vol. 21, no. 7, pp. 786–800, Jul. 2002.
- [46] Z. Wang, A. C. Bovik, H. R. Sheikh, and E. P. Simoncelli, "Image quality assessment: From error visibility to structural similarity," *IEEE Trans. Image Process.*, vol. 13, no. 4, pp. 600–612, Apr. 2004.
- [47] X. B. Song, A. Myronenko, S. R. Plank, and J. T. Rosenbaum, "Registration of microscopic iris image sequences using probabilistic mesh," in *Medical Image Computing and Computer-Assisted Intervention—MICCAI*, vol. 4191. New York, NY, USA: Springer, Oct. 2006, pp. 553–560.
- [48] F. Zana, I. Meunier, and J. C. Klein, "A region merging algorithm using mathematical morphology: Application to macula detection," in *Proc. ISMM*, 1998, pp. 423–430.
- [49] Z. Ghassabi, J. Shanbehzadeh, A. Sedaghat, and E. Fatemizadeh, "An efficient approach for robust multimodal retinal image registration based on UR-SIFT features and PIIFD descriptors," *EURASIP J. Image Video Process.*, vol. 2013, no. 1, pp. 1–16, 2013.
- [50] I. F. Talos and N. Archip, "Volumetric non-rigid registration for MRI guided brain tumor surgery," Dept. Radiol., Brigham Women's Hospital, Harvard Med. School, Surgical Planning Lab., Boston, MA, USA, Tech. Rep., Aug. 2007. [Online]. Available: <http://www.spl.harvard.edu/publications/item/view/541>
- [51] W. R. Brody, "Digital subtraction angiography," *IEEE Trans. Nucl. Sci.*, vol. NS-29, no. 3, pp. 1176–1180, Jun. 1982.